PART II

Realization of Experimental Set-ups and Interpretation of Measurements

Chapter 9

Torsion Test Benches: Instrumentation and Experimental Results

9.1. Introduction

The theoretical aspects of the torsional vibration of rods are presented in detail elsewhere, with special attention to the problem of cross-section warping [CHE 10; Chapter 5].

In this chapter, special apparatus are presented with two different objectives. The first concerns a torsional test bench which is easy to use. It serves to quickly characterize elastic and/or viscoelastic materials in the lower frequency range (up to approximately 400 Hertz) for industrial applications.

The other class of apparatus is conceived and realized in such a manner that it permits the exploration of the largest range of frequencies, up to ultrasonic frequencies (of the order of 100,000 Hertz) so as to obtain a dispersion curve, i.e. wave velocity versus frequency. Given the large frequency range being taken into account, the instrumentation is naturally not the same as in a test bench realized for industrial purposes.

9.2. Industrial torsion test bench

9.2.1. *Mechanical parts of the apparatus*

Before presenting details of the various mechanical parts, it is useful to sketch the main ideas. Our objectives are:

Chapter written by Michel NUGUES.

Mechanical Characterization of Materials and Wave Dispersion: Instrumentation and Experiment Interpretation
Edited by Yvon Chevalier and Jean Tuong Vinh

– to adopt a sample holding system which is easy to manipulate, with simple boundary conditions which are easy to realize;

– if possible, to apply torque at the clamped end so as to obtain all levels of excitation signal, and to use an electrodynamic shaker;

– to choose boundary conditions which avoid sample length correction, such as the classical clamping presented in Chapter 3, section 3.6.1;

– to choose a pair of contactless transducers (see Chapter 5, sections 5.5.2 and 5.5.3) to minimize their possible non-linearities.

Figure 9.1 presents a general assembly drawing. Details of various parts of the mechanical apparatus are described below. Closely built-up apparatus with the same functions can be used, for example see Renard [REN 05], Chapter 8.

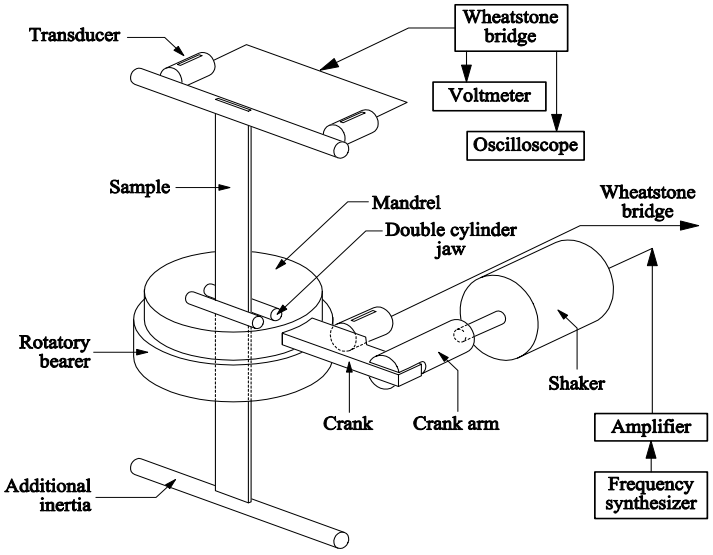

Figure 9.1. *Schematic drawing of the apparatus used for torsion tests*

9.2.1.1. *Shaker and crank system*

With the sample being in a vertical position, the shaker is fixed horizontally on a rigid platform so that its axis is connected to the mandrel via a system constituted by the crank arm and the crank itself.[1]

1 The adoption of vertical position for the sample allows a reduction in the rod bending effect, due to additional inertia at both ends.

9.2.1.2. *Sample holder system*

A pseudo-clamping system is adopted (see Chapter 3, section 3.6.1) which allows the sample to be maintained in a vertical position. The jaw, made up of two steel cylinders, has the following advantages: it does not necessitate sample length correction and requires only a moderate clamping force compared to classical sample clamping between flat plates. The symmetrical disposition of the sample contributes to maintaining the sample in its position, without any slipping between the jaws and the sample.

9.2.1.3. *Mandrel and rotary bearer*

A mandrel with a key allows clamping force to be applied through the two cylinder jaws. A torque dynamometer is used to measure the tightening force. The function of the rotary bearer is to guide the alternative rotation of the sample. Utilization of ball bearings is to be avoided: the alternative rotary motion might produce an impact between balls and this creates a noise response for the transducers. The inner side of the rotary bearer has a special self-lubricating ring.

9.2.1.4. *Fixing of additional rotary inertia at both sample ends*

The role of the additional rotary inertia at both sample ends is to contribute to a mechanical amplification of torsion angles at the free ends, and also to maintain working frequencies in lower range.

9.2.1.5. *Device to obtain exact length of each half of the sample*

The whole set (mandrel, sample, additional inertias) must be adjusted to ensure that the two halves of the sample are of exactly equal length. This symmetry is obtained before installing the mandrel in the apparatus. First the mandrel is maintained in a vertical position so as to permit the sample to be in horizontal equilibrium. The distance between the cylinder jaws is increased so as to create an air gap. The equilibrium of the sample is adjusted whilst it is in contact with only one jaw cylinder. The sample equilibrium is obtained not only for the two half lengths of the sample but also for its perpendicular position with respect to the cylinder jaws, before applying the clamping force with a special key.

9.2.2. *Electronic set-up*

9.2.2.1. *Shaker*

The size of the shaker is related to the available power. The mechanical system represented above imposes a severe regime to the shaker. An electrical output power of 25–50 Watts is necessary to avoid damage being imposed on the moving coil.

9.2.2.2. *Power amplifier*

A power amplifier (of approximately 100 Watts) should be chosen from a range of power amplifiers for high fidelity acoustic systems. However, an amplifier with an electronic breaker at the output stage should be selected, so as to prevent a sudden electric shock being imposed to the moving coil.

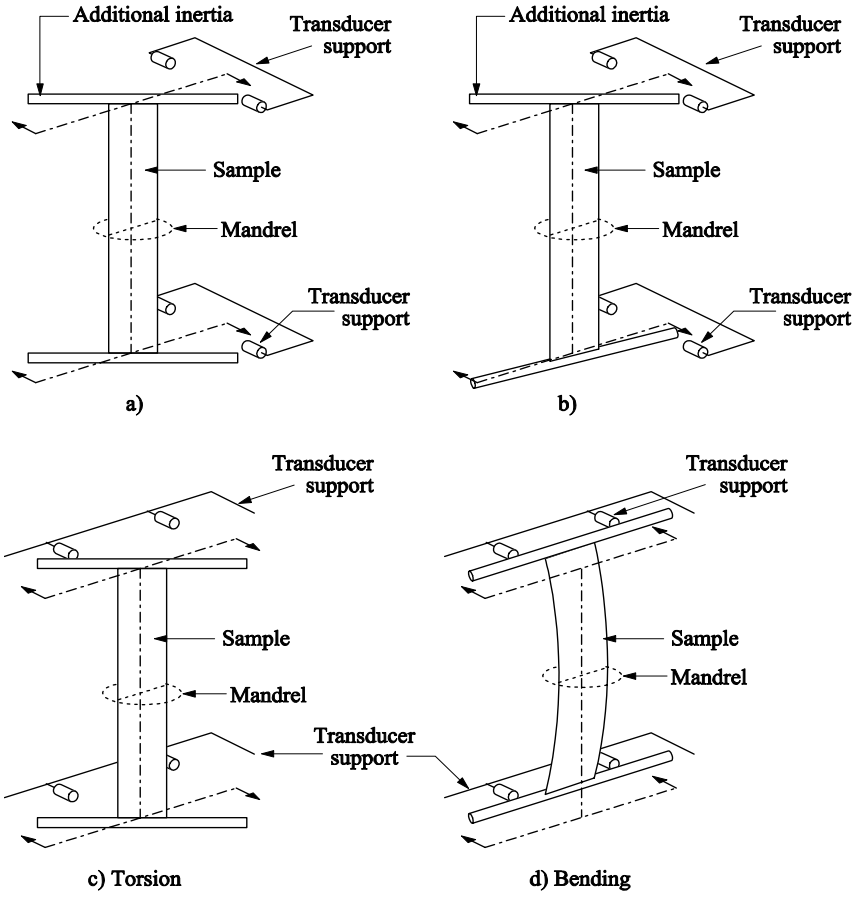

Figure 9.2. *Sample mounting with two additional inertias. Transducers are mounted by pairs at both ends and in the middle: (a) good sample centering; (b) defective sample centering; (c) torsion; (d) parasitic bending vibration. The detection of torsional and bending vibrations can be made with transducers at one sample end and visual observation of the relative phase between vibrations*

9.2.2.3. *Signal generator and frequency synthesizer*

Two signal generators can be used. The first serves for quick adjustment of the resonance sample frequency. The second generator, driven by a quartz oscillator with digital visual display, is used for the accurate frequency measurement ($\Delta f \cong 10^{-3}$ Hertz).

9.2.2.4. *Amplitude control of input signal*

The amplitude control of the input signal in the middle of the sample can be obtained by an appropriate industrial apparatus. This is useful when we have to deal with a low damping sample.

9.2.2.5. *Automatic frequency sweeping velocity*

This automatic frequency sweeping velocity is inversely proportional to the damping capacity of the sample (see Chapter 4).

9.2.2.6. *Transducers*

A displacement-type transducer (inductive or eddy current transducer) should be chosen. If possible, for input and output signals, a pair of transducers for each signal is preferred. A preliminary calibration of each set of transducers is necessary.

9.3. Parasitic bending vibration of rod

If torsional vibration is recorded over a large range of frequency, it is possible that a defect in the mounting of the rod might have created parasitic bending vibration. Possible defects in rod vibration are presented in Figure 9.2(d). This is due probably to defective centering of the sample in the mandrel. Bending vibration gives rise to oscillations which are in phase at the four ends of the additional inertias, compared to the pure torsional oscillations presented in Figure 9.2(c).

9.4. Shear moduli of transverse isotropic materials

If Cartesian coordinates are adopted, axis 3 should be along the fiber direction of a composite material, and axes 2 and 3 in the isotropic plane. Two shear moduli, $G_{23} = G_{13}$ and G_{12}, are to be evaluated.

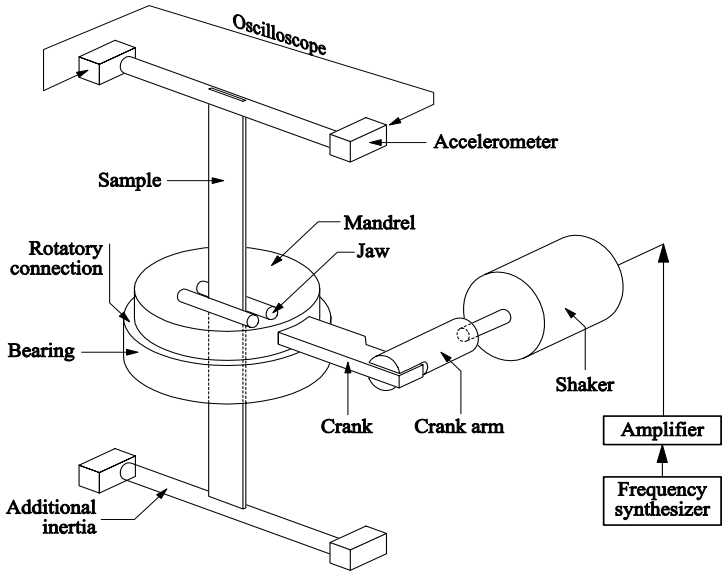

Figure 9.3. *Set-up to record sample response over a large range of frequency by using accelerometers. Observation of oscillations are made at both ends of the oscilloscope*

Figure 9.4 shows two samples cut from composite plates. G_{12} corresponds to Figure 9.4(b). The sample in this figure is fragile and precautions must be taken to avoid sample breaking.

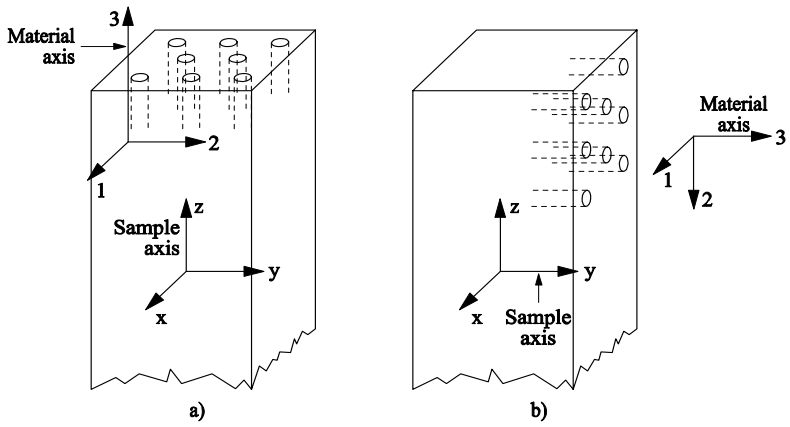

Figure 9.4. *Transverse isotropic material: 3 is the isotropic axis; 1 and 2 are the two axes in the isotropic plane. (a) Sample with axis Oz is coincident with the material axis 3; (b) sample with axis oz perpendicular to axes 1 and 3*

9.4.1. *Shear moduli by elementary theory*

This theory is presented in details elsewhere ([CHE 10], Chapter 5).

9.4.1.1. *Eigenequation*[2]

$$\rho L I_p / J_a = \zeta \tan\zeta \qquad [9.1]$$

where ρ is the material density, L the half length of the sample, I_p the polar surface inertia, and J_a the additional torsional inertia at z=L.

Remember that the eigenvalue δ is used to express the torsional angle θ (z,t), z being the coordinate along the sample axis:

$$\theta(z,t) = \exp(j\omega t)\,[\,A\cos(\zeta z/L) + B\sin(\zeta z/L)] \qquad [9.2]$$

The torsional stiffness is:

$$C_T = L J_a \omega^2 (\tan\zeta / \zeta) \qquad [9.3]$$

As in [9.1], the first member is small:

$$\gamma = \rho L I_p / J_a << 1 \qquad [9.4]$$

With limited expansion of the series representing tan δ, [9.3] is rewritten as:

$$\rho L I_p / J_L = \gamma \cong \delta(\delta + \delta^3/3)$$

Then, from [9.3], the stiffness is:

$$C_T \cong L J_a \omega^2 (1+\zeta^2/3) \text{ or } C_T \cong L J a \omega^2 (1+\gamma/3)$$

2 See Appendix 9A for further information concerning these formulae.

though this approximation is valid only for the first mode of vibration. In the general case, [9.3] can be solved by an iterative program using Newton's method giving all the modes.

9.4.1.2. *Expression of shear modulus G_{yz}*

Two cases are distinguished:

(a) Sample axis z coincident with the material's isotropic axis 3

The formula giving G_{xz} is:

$$C_T = G_{yz}\, hb^3 \beta_T(c) = G_{xz}\, bh^3 \beta_T(1/c) \quad [9.5]$$

$$\text{with: } c = \frac{h(thickness)}{b\ (width)} \sqrt{\frac{G_{xz}}{G_{yz}}} \quad [9.6]$$

As $G_{yz} = G_{xz}$, c is reduced to $c = \frac{h}{b}$

$\beta_T(c)$ is given by the series presented in Appendix 9C.

Then:

$$G_{yz} = G_{23} = G_{13} = \frac{C_T}{hb^3 \beta_T(c)} = \frac{J_a L\omega^2 (1+\frac{\gamma}{3})}{hb^3\ \beta_T(c)} \quad [9.7]$$

(b) Sample axis coincident with axis 1 or 2 (Figure 9.4(b))

The formula is given above in [9.5]; the difference between this and case (a) above is that the two shear moduli under the square root are not equal:

$$c = \frac{h(thickness)}{b\ (width)} \sqrt{\frac{G_{12}}{G_{23}}} \quad \text{with } \frac{G_{12}}{G_{23}} \neq 1 \quad [9.8]$$

From [9.8] we write:

$$\beta_T(c) = \frac{C_T}{(G_{23} = G_{yz}) hb^3} \quad [9.9]$$

in which G_{23} is as previously evaluated in the sample presented above in Figure 9.4. The intermediate parameter is c, equation [9.5]:

$$c = \frac{h}{b}\sqrt{\frac{(G_{12}=G_{xz})}{(G_{23}=G_{yz})}} \qquad [9.10]$$

c is then evaluated when $\beta_T(c)$ is calculated from [9.9]. From c, G_{12} is deduced, G_{23} being known. The successive operations are different to those in case (a) previously presented. The parameter $\beta(c)$ versus c is given in Table 9C.1.

$$\text{Then: } G_{xz} = G_{12} = G_{23}\frac{c^2b^2}{h^2} \qquad [9.11]$$

Interpolating, using Table 9C.1, $\beta_T(c)$ must be effected with enough accuracy for the c value.

In equation [9.6] the variable c depends on the flatness ratio δ of b (width) to h (thickness). If too large a ratio is chosen, there is a problem. In Figure 9.5, variable c can have a large value and the curve $\beta_T(c)$ is nearly in the horizontal asymptotic region. If possible, a small ratio h/b is selected.

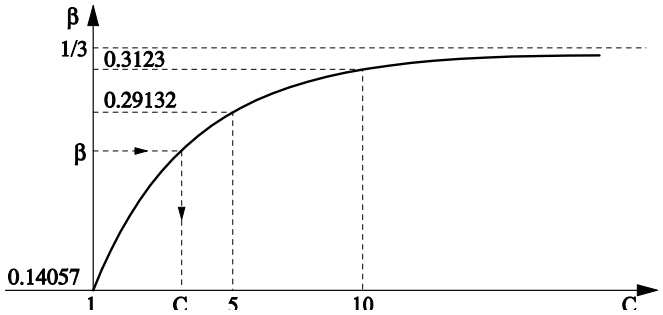

Figure 9.5. *c is estimated from the value $\beta_T(c)$ calculated by equation [9.C.3]*

9.4.2. *Shear moduli by higher approximation equation of motion*

In the elementary equation of motion a simple field of displacement is adopted. We have two unknown functions to evaluate: the torsion angle $\theta(z,t)$ and the warping function $\phi_w(x,y)$ which can be solve as a static problem. For higher approximation, we cannot hypothesize that the axial displacement w(z,t) is dependent only on the torsion angle α and the function ϕ_w .

ϕ_w. $\theta(t)$ is replaced by a function of two variables as follows:

$$w(z,t) = \xi\,(z,t)\,\phi_w(x,y) \qquad [9.12]$$

We can formulate the equations of motion by using Hamilton's principle. The result is that we have to deal with two equations of motion of second order with coupled terms. Using the substitution method, we obtain a differential equation of one unknown variable of the fourth order. Details of the solving of this equation can be found elsewhere (see [CHE 10, Chapter 5]).

Young's modulus is obtained by a complementary bending test, see Chapter 10.

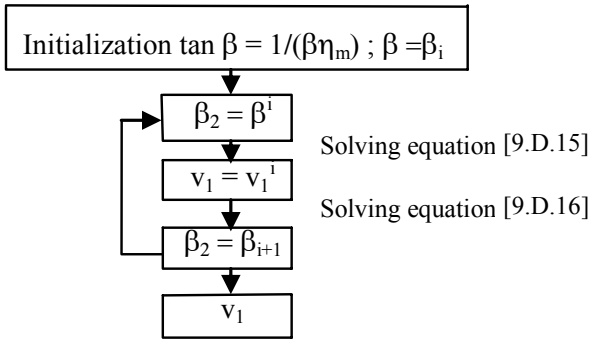

Figure 9.6. *Solving a couple of equations using trigonometric and hyperbolic functions to obtain higher order eigenvalues (for [9.D.15] and [9.D.16] see Appendix 9D)*

9.5. Elastic moduli obtained for various materials

Five materials were tested: steel, brass, unidirectional glass-fiber composites with epoxy resin matrix and phenolic resin matrix and Kevlar. Let us mention that with higher order approximation theory of vibration, shear moduli obtained are sensibly different from the value using elementary theory. Tables 9.1 and 9.2 present data, measurements and elastic moduli. Table 9.3 presents the torsional eigenfrequencies at different modes. The two theories (elementary and higher order theories) are used to predict eigenfrequencies which are compared to experimental values.

For metallic materials, discrepancies between the theories are weak. For composite materials, higher order approximation theory gives better results and

estimated eigenfrequencies approach experimental ones particularly for higher modes.

Data and measures	Steel	Brass	Glass fiber-epoxy resin		Glass fiber-phenolic resin (Long.)	Kevlar (Long.)
			(Long.)	(Trans.)		
$b.10^{-3}$ m	10.4	10.1	8.15	7.66	8.85	9.85
$h.10^{-3}$ m	1	1.01	0.8	4.25	1.34	3.8
$2L.10^{-3}$ m	181	211	188	137	140.4	150
$L_u.10^{-3}$ m	84.5	99.5	88	62.5	64.2	69
$\rho.10^3$ Kg/m^3	7.531	8.226	1.983	2.006	2.013	1.102
β (c)	0.313133	0.312325	0.312711	0.182752	0.301524	0.252332
$P_1^*.10^{-18}$ m^6	7.496	7.051	1.844	24.587	10.481	199.54
f Hz (bending)	102.9	52.3	77	437	213	730
f Hz (torsion)	166.2	102	31.2	336	7.97	134.7

Table 9.1. *Data and measurements for five materials. Asterisk* (*) *designates modulus obtained with higher order approximation theory of motion. 2L = full sample length, L_u = useful sample half length. Long. = longitudinal: sample axis collinear with material axis; Trans. = transverse: rod axis z perpendicular to material axis 3*

Data and measures (Young's moduli)	Steel	Brass	Glass fiber-epoxy resin		Glass fiber-phenolic resin		Kevlar (Long.)
			(Long.)	(Trans.)	(Long.)	(Trans.)	
E_{33} (10^7 Pa)	20535	10455	5469		4724		4933
E_{11} (10^7 Pa)				1802		1842	
G_{13} (10^7 Pa)	8729	3887	796		769		111
G_{13}^* (10^7 Pa)	8491	3788	768		738		101
G_{12} (10^7 Pa)	8729	3887		452		412	
G_{12}^* (10^7 Pa)	8491	3788		474		471	

Table 9.2. *Tests on five materials. Young's moduli are measured on another bending test bench. Asterisk* (*) *designates modulus obtained with higher order approximation theory of motion. Long. = longitudinal: sample axis collinear with material axis; Trans. = transverse: rod axis z perpendicular to material axis 3*

Material	Frequency per mode rank (Hz)	Saint Venant's method (Hz)	Higher approximation (Hz)	Experimental data (Hz)
Steel	f_1	29.4	29.8	29
	f_2	3686	3802	3726
	f_3	7372	7684	7608
	f_4	1108	11752	-
Brass	f_1	17	17.2	16.4
	f_2	1951	2008	2012
	f_3	3902	4045	4109
	f_4	5853	6185	6257
Glass fiber phenolic resin Transverse	f_1	80	60.3	f_1=58.5
	f_2	11423	11491	
	f_3	22846	23013	
	f_4	34269	34596	
Glass fiber-epoxy resin Longitudinal	f_1	5.5	5.6	5.6
	f_2	2117	2207	2197
	f_3	4234	4492	4780
	f_4	6351	6933	7297
Kevlar fiber-epoxy resin Longitudinal	f_1	23	24.1	f_1= 24
	f_2	4348	4987	f_2=5110
	f_3	8697	10789	
	f_4	13046	18363	

Table 9.3. *Confrontation theories (Saint Venant's and higher approximation theories) and experiments on various materials*

9.6. Experimental set-up to obtain dispersion curves in a large frequency range

In the experimental set up presented in Figure 9.1, we used an electrodynamic shaker which is adapted for low frequency excitation ($10 < f < 5{,}000$ Hz). If the frequency range is extended to higher frequency (say $f \cong 100{,}000$ to $300{,}000$ Hertz) this shaker should be replaced by a piezoelectric exciter or contactless inductive exciter.

9.6.1. *Rod suspension and instrumentation*[3]

As long a sample as possible is chosen so as to obtain the lowest eigenfrequencies. Additional inertias at both ends are to be avoided because they favor a lower working frequency and are an energy consumer to the detriment of higher frequencies. The best system to adapt is the free-free rod with piezoelectric exciter and a transducer as light as possible with respect to the rod mass. This

3 This section is extracted from [ONO 78].

problem was presented in Chapter 3. Figure 9.7 shows a rod suspended by two nylon yarns. To prevent parasitic lateral rod vibration, two pairs of yarns are proposed. As stationary torsional vibrations are adopted, anti-symmetrical exciters are used to prevent parasitic bending vibrations.

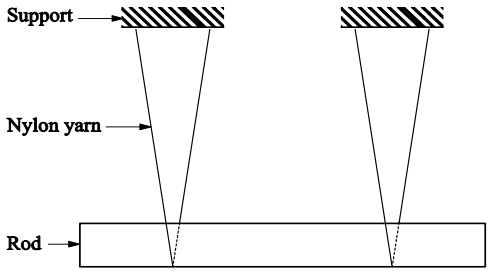

Figure 9.7. *Two nylon (or cotton) yarns are used to suspend a long rod*

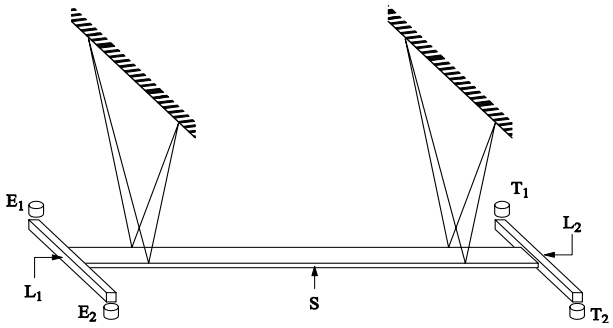

Figure 9.8. *Contactless magnetic exciters are disposed anti symmetrically with respect to the steel short lever so as to produce torsional vibrations on the sample S. The gaps between E_1 and E_2 (exciters) and T_1 and T_2 (transducers) must be adjusted so as to obtain the same sensitivities for both exciters and transducers. Two pairs of strings are used to prevent parasitic lateral motion of the sample*

9.6.2. *Electronic set-up*

We should mention that the use of two pairs of transducers necessitates multi-entrance oscilloscopes in Figure 9.9 by observation of in-phase (bending) and anti-phase (torsional) oscillations of transducers and exciters.[4]

4 In bending tests, in Figure 9.9, the excitation signals E_1 and E_2 are in phase. So are the signals T_1 and T_2 representing the response of the bar. I torsion tests, exciter signal E_1 and E_2 must be in phase opposition. The signals T_1 and T_2 are also in phase opposition.

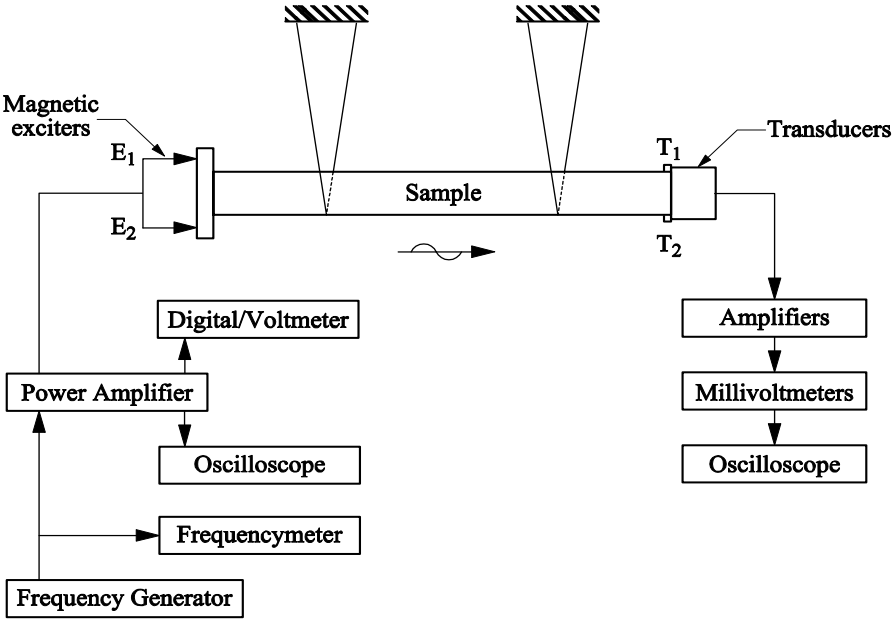

Figure 9.9. *Basic view of electronic set-up*

9.7. Experimental results obtained on short samples

The weight of the two steel levers and their inertias is small compared to the sample weight and inertia; the sample can be considered as free-free rod. This considerably eases the calculations. The utilization of a pair of transducers permits the difference between torsional vibrations and parasitic bending vibrations to be distinguished as indicated in footnote 4.

Appendix 9B presents Onobiono's contribution concerning the eigenfrequencies of torsional rod vibrations.

The objective of this section is twofold:

– to check the validity of dynamic torsion theories: Saint Venant's theory and Engstrom's generalized theory extended to composite materials;

– to take measurements of more than ten eigenfrequencies by resonance tests.

9.7.1. *Checking the validity of Saint Venant's theory and Onobiono's theory on isotropic material*

9.7.1.1. *Test on steel ADXE*

Table 9.4 presents results concerning steel ADXE. The flatness of the sample being large ($\delta = \frac{b(width)}{h(thickness)}$ = 2), phase velocity varies with frequency and the relative error e_2 can reach 7%, while the relative errors e_1 are of the order of 3%. The length L= 0.199m, width b= 0.0198m, thickness h= 0.0099 m, ρ density = $7.819.10^{-3}$ kg/m^3, additional masses m_1= 0.0085 kg, m_2 = 0.0027 kg.

J (mode rank)	$\mathbf{f_M}$ (Hz)	$\mathbf{f_C}$ (Hz)	$\mathbf{f_{SV}}$ (Hz)	$\mathbf{e_1}$ (error)	$\mathbf{e_2}$ (error)
1	3688	3720	3731	0.0086	0.0115
2	7214	7309	7342	0.0129	0.0174
3	11845	11905	11953	0.0050	0.0090
4	15692	15828	16029	0.0085	0.0210
5	21410	21967	22318	0.0253	0.0406
6	26222	26823	27412	0.0224	0.0434
7	30094	31020	32225	0.0298	0.0661
8	36945	37456	38825	0.0136	0.0484
9	48729	49826	51425	0.0220	0.0524
10	53628	54416	55902	0.0144	0.0406
11	59049	60128	63488	0.0179	0.0699
12	65125	67011	70002	0.0281	0.0696
13	73420	76338	79498	0.0382	0.0764

Table 9.4. *Results for ADXE steel. j is the rank of eigenfrequency, f_M is the measured frequency, f_C is the calculated eigenfrequency from Onobiono's theory, f_{SV} the calculated eigenfrequency from Saint Venant's theory, e_1 and e_2 relative discrepancies between (f_M and f_C) and (f_M and f_{SV})*

9.7.1.2. *Test on glass – epoxy resin composite*

Sample length L= 0.179 m, width b=0.0192, thickness h= 0.00384m, density ρ= $1.869.10^{-3}$ kg / m^3, additional masses: m_1 = 0.0032kg , m_2 = 0.0027kg, Flatness δ = 5.

The frequency range was extended to the 12th mode. The discrepancy obtained for e_2 was 7%, while e_1 is of the order of 2%.

J (rank)	f_M (Hz)	f_C (Hz)	f_{SV} (Hz)	e_1	e_2
1	3133	3325	3510	0.0577	0.1074
2	6486	7345	7888	0.1169	0.1777
3	10113	11841	12695	0.1459	0.2033
4	14118	15241	16498	0.0736	0.1442
5	18047	19246	19866	0.0736	0.0915
6	23907	24401	25708	0.0622	0.0700
7	27853	29941	30025	0.0697	0.0723
8	30449	32383	32879	0.0597	0.0739
9	35540	36442	37272	0.0247	0.0464
10	40177	42317	45028	0.0505	0.1077
11	49170	52306	55823	0.0599	0.11191
12	53806	58998	63628	0.0864	0.1543

Table 9.5. *Tests on composite glass fiber-epoxy resin. f_M is the measured eigenfrequency; f_C the eigenfrequency estimated using Onobiono's theory, f_{SV} the eigenfrequency estimated using Saint Venant's theory. Length L= 0.179m, Width b= 0.0192, Thickness h= 0.0038m, density $\rho=1.869.10^{-3}$kg/m, Additional masses: $m_1 = 0.0032$kg, $m_2 = 00027$kg*

9.7.2. *Remarks on elastic characterization of materials with torsion tests*

Isotropic metallic materials currently have elastic moduli which vary weakly with frequency. The viscoelastic behavior of such materials at ambient temperature gives rise to a damping coefficient in the range (10^{-3}–10^{-2}). If experiments are confined to low eigenfrequencies (see Tables 9.4 and 9.5), the relative errors with respect to experiments are of the order of 1–2% and Saint Venant's theory is acceptable.

Composite materials. The two main parameters to retain when evaluating the performance of composite materials are:

Flatness $\delta = \frac{width\ b}{thickness\ h}$. Flatness has a strong influence on the wave dispersion in isotropic materials and also on composite materials. In order to reduce the influence of a large flatness coefficient, and if the experimenter has a latitude of choice, a square cross-section is preferred. This cross-section gives rise to a dispersion curve which approaches the ideal circular section.

Ratio $\frac{E_3\ Young's\ modulus}{G_{13} or\ G_{23} shear\ modulus}$, 3 in the subscripts indicates the direction of the fibers in transverse-isotropic materials.

For isotropic materials (metallic) the upper limit for this ratio is 3 while for anisotropic materials, this ratio reaches 40 to 50, which explains the trend of

dispersion curves in which wave velocity strongly varies with frequency before reaching a horizontal asymptote.

The important conclusion we can retain is that, if one wants to characterize composite materials in shear, by using dynamic methods at medium and high frequency, it is important to refer to higher approximation equations of motion.

Table 9.5 shows, at medium frequency, that the relative error is of the order 15% for Saint Venant's theory, while Onobiono gives rise to 8% as an upper limit.

9.8. Experimental wave dispersion curves obtained by torsional vibrations of a rod with rectangular cross-section

In the preceding section, torsional dynamic tests were used to evaluate shear moduli of isotropic and anisotropic materials. For this purpose, rods with short length are used. With these kinds of test, the phase velocity is evaluated via the resonance frequency of the sample.

If one wants to draw the experimental dispersion curve concerning phase velocity, the objective is then to obtain the greatest number of eigenfrequencies as possible so as to cover a large range of frequency (or wave numbers). The rod adopted for this experiment must be as long as possible. The measured eigenfrequencies must be less dependent on boundary conditions imposed at both ends. If we look back to the experimental set-ups in Figures 9.7 and 9.8, we notice that the additional masses or inertias imposed at both ends complicate the calculation by adopting (for displacement components in the rod) normal functions. In the eigenvalue equations, transcendental functions are used.

Consequently the adopted boundary conditions are often those with free ends. Taking into account the excitation sources and the measurement of vibration amplitude by transducers, the additional metallic weights at both ends (bending test) or additional inertia (torsion test) must be small compared to the weight of the rod.

$$\frac{m\ (additional\ weight)}{M\ (rod\ mass)} \text{ or } \frac{J_a\ (additional\ inertia\ in\ torsion\ )}{I\ (inertia\ of\ the\ rod\ in\ torsion)} << 1 \quad [9.13]$$

If this inequality is satisfied we can say that, when a resonance occurs, the rod length L is related to the wavelength λ_n of order n by:

$$L = n\,\lambda_n/2 \text{ or } \lambda_n = 2L/n \quad [9.14]$$

where n is a positive integer.

The velocity is then:

$$v_n = \frac{2L}{n} \cdot f_n \quad [9.15]$$

Introducing the wave number k_n:

$$v_n = \frac{2\pi}{k_n} f_n \quad [9.16]$$

Adopting a dimensionless phase velocity as:

$$\bar{v} = \frac{v_n}{v_0} \quad [9.17]$$

where v_0 is equal to $2Lf_1$, f_1 being the fundamental resonance frequency.

With h being the thickness, the dimensionless wave number is:

$$\bar{k}_n = k_n .h/2 \quad [9.18]$$

9.8.1. *Dispersion curves of metallic rods with rectangular cross-section*

For each of the rods below, 150 resonance frequencies were detected and measured. Detection beyond 100,000 Hz of resonance frequency becomes difficult.

9.8.1.1. *Aluminum alloy AU4G*

The dimensions of the sample are given below. AU4G is the reference of aluminum fabricated in France.

L = 1.719m, b (width) = 14.9 x 10^{-3} m, h (thickness) = 14.9 x 10^{-3} m (square cross-section), flatness $\delta = 1$.

9.8.1.2. *French aluminum alloy AU4G*

The sample has the following dimensions:

L= 1.719 m, b = 19.8.10^{-3}m, h= 9.9.10^{-3}m (rectangular cross-section); flatness $\delta = 2$.

9.8.1.3. *Steel ADXE*

L= 1.194 m, b= 11.8 x 10^{-3} m, h = 11.8 x 10^{-3} m (square cross-section); flatness $\delta = 1$.

9.8.1.4. *Steel ADXE*

L=2.1m b= 20 x 10^{-3}m, h= 10 x 10^{-3} m (rectangular cross-section); flatness δ =2.

Figure 9.10 presents dispersion curves for the two aforementioned materials.

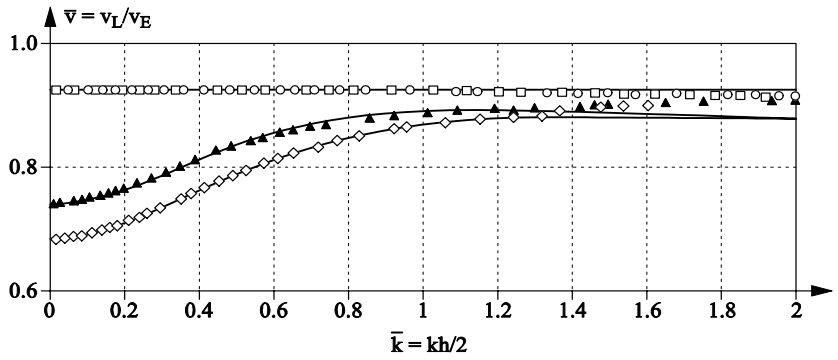

Figure 9.10. *Experimental dispersion curves of isotropic metallic rod (aluminum and steel). Only the first branch is represented.*
▲ *= rod with rectangular cross-section – aluminium;*
◊ *= rod with rectangular cross-section – steel;*
□ *= rod with square cross-section – aluminium;*
○ *= rod with a square cross-section – steel;*
$\bar{v}$ *is the dimensionless velocity and* $\bar{k}$ *the dimensionless number*

For the square section, the first branch of elastodynamic mode corresponds to a horizontal line with a small decrease at a high value of waves number $\bar{k}$.

For a rectangular cross-section, for both materials, the dispersion is pronounced.

9.8.2. *Dispersion curves of anisotropic materials*

(a) Rod with square section: composite material with long glass fiber–polyester resin as matrix:

L= 1,750 m, b= 11.8 x 10^{-3} m, h= 11.8 x 10^{-3} m

(b) Rod with rectangular cross-section: composite with long glass fiber–polyester resin as matrix:

L= 1,435 m, b= 18.8 x 10^{-3} m, h= 9.4 x 10^{-3} m, flatness coefficient δ= 2

The frequency range extends from 30 Hertz to 60 KHertz. The energy level necessary to obtain detectable resonances is higher than for metals.[5]

The elastic coefficients of the stiffness matrix of the composite (fiber glass–polyester resin) are:

C_{1111} = 1726 x 10^7 Pa; C_{1212}= 381 x 10^7 Pa ; C_{1313}= 502 x 10^7 Pa;

C_{3333}= 4256 x 10^7 Pa; C_{2323}= 586 x 10^7Pa;

Density $\rho = 2.0008 \times 10^3$ kg/m^3.

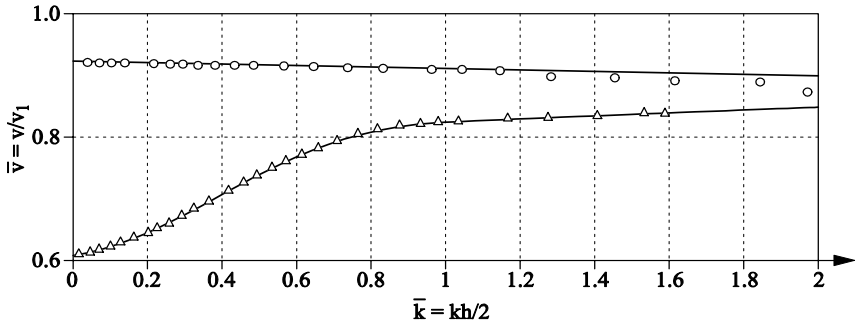

Figure 9.11. *Experimental dispersion curve of composite material (glass fiber–polyester resin). Dimensionless velocity* $\bar{v} = \frac{v}{v_1}$ *= versus dimensionless wave number* $\bar{k} = \frac{kh}{2}$, *h thickness. O = square cross-section; Δ = rectangular cross-section. The rectangular cross-section corresponds to the flatness coefficient δ=2*

9.9. Frequency spectrum for isotropic metallic materials (aluminum and steel alloy)

The elastodynamic spectrum[6] must be understood as a representation of an elastodynamic curve in the circular frequency ω versus wave number k plane. If k is complex, it does not necessarily mean that the material is viscoelastic. Rather, viscoelasticity corresponds to the complex value of k obtained after calculation.

5 Inductance transducers are used in the experimental set-up. If higher resonance frequencies are to be exploited, special piezoelectric transducers are necessary; see Chapter 15.

6 This spectrum must not be confused with the spectrum currently used in digital signal processing.

Figure 9.12 concerns two metallic materials already presented above (steel and aluminum alloy). The curves are presented with real values of k. Figure 9.13 concerns composite materials (glass fiber with polyester resin as a matrix). For a rod with a rectangular section, the curve departs from the straight line. This means that, in the region of circular frequency explored, there is a weak dispersion.

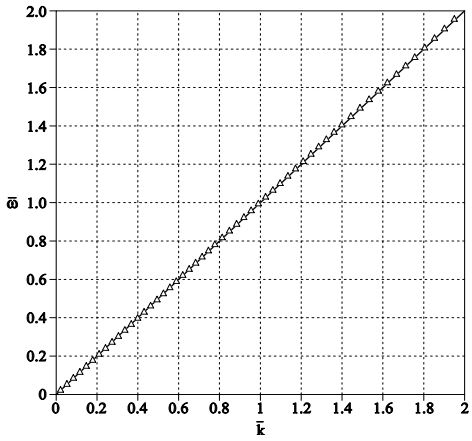

Figure 9.12. *Elastodynamic spectrum concerning steel and aluminum alloy, where $\bar{\omega}$ is the reduced circular frequency, and $\bar{k}$ the reduced wave number. Δ and O correspond to experimental values; the continuous line corresponds to theory*

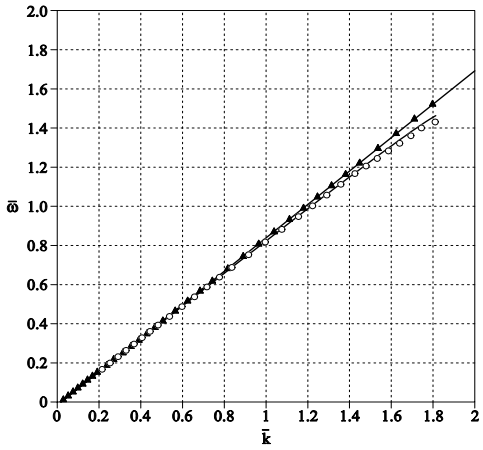

Figure 9.13. *Elastodynamic spectrum (real branch) first mode (composite material: glass fiber–polyester resin), where $\bar{\omega}$ is the reduced circular frequency, and $\bar{k}$ the reduced wave number. ▲ is the square cross-section, O rectangular cross-section with flatness δ=2 reduced circular frequency*

Figure 9.13 shows composite materials; the departure from the straight line is perceptible for relative wave numbers exceeding 1.3.

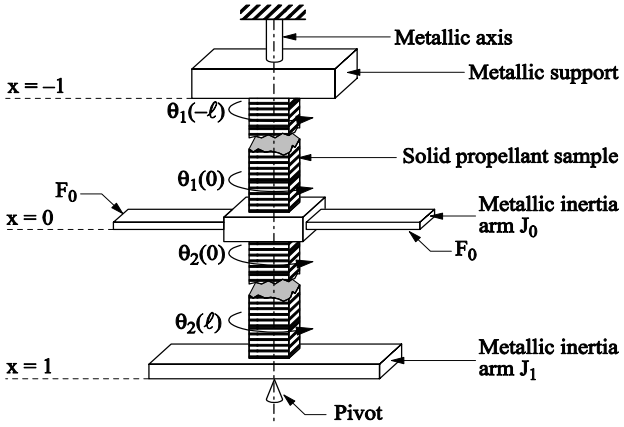

Figure 9.14. *Sketch of experimental set-up. The sample (with a square cross-section) is glued to the upper support in a vertical position. The inertia arm is fixed to the middle of the sample. Additional inertia is fixed at lower free end*

9.10. Impact test on viscoelastic high damping material

The problem treated in this section concerns a solid propellant whose damping coefficient is high and for which dynamic tests must be carried out in the minimum of time so as to avoid temperature change. The impact test is chosen for this reason but also because of the viscoelastic characteristics of this special material itself. The peak amplitude of the impact force produced by a hammer may be high. When exploring the behavior of this material in the region called the temperature transition zone, the damping coefficient is unusually high: $\tan \delta_G \approx 0.2–4$.

Figure 9.14 shows a sketch of the experimental set-up. The impact force created by a special hammer is applied to the metallic lever at the middle of the sample. To avoid parasitic bending vibration, the lower additional inertia level has a guiding pivot. The upper metallic support is connected to a vertical metallic axis.

9.10.1. *Solution of the viscoelastic problem*

As the damping coefficient of a solid propellant is high, the forced dynamic vibrations of the sample are confined to the lower range of frequency. Elementary torsion theory is referred to. The principle of correspondence is invoked to obtain a

close form viscoelastic solution from an elastic solution with the same boundary conditions [CHE 10].

As we have to deal with a high damping viscoelastic material and the explored frequency range is up to 100 Hz, an elementary equation of motion is adopted:

$$C_T^* \frac{\partial^2 \theta}{\partial z^2} = \rho I_p \frac{\partial^2 \theta}{\partial t^2} \quad [9.19]$$

Boundary conditions for the additional inertias arms are:

$$\left.\begin{array}{ll} z = -L & \theta_1(-L,t) = 0 \\ z = 0 & \theta_1(0,t) = \theta_2(0,t) \\ & J_0 \dfrac{\partial^2 \theta}{\partial t^2} = -C_T \left(\dfrac{\partial \theta_1}{\partial z} + \dfrac{\partial \theta_z}{\partial z} \right) + M(t) \\ z = L & J_L \dfrac{\partial^2 \theta_2}{\partial t^2} = -C_T \dfrac{\partial \theta_2}{\partial z} \end{array}\right\} \quad [9.20]$$

Indexes 1 and 2 designate the rotation angle at the upper and lower parts of the sample respectively.

$$\text{Let } s^* = \pm \left[\frac{p^2 \rho I_p}{C_T^*} \right]^{1/2} \quad [9.21]$$

where p is a complex Laplace variable.

The Laplace transform of $\theta(z,t)$ is:

$$\theta^*(p,z) = \int_0^\infty \theta(t,z) e^{-pt} dt \quad [9.22]$$

We try a solution for $\theta^*(p, z)$ under the form:

$$\theta_1^*(p,z) = A(p) \cosh s^* z + B(p) \sinh s^* z$$

$$\theta_2^*(p,z) = C(p) \cosh s^* z + D(p) \sinh s^* z \quad [9.23]$$

Taking into account the boundary conditions [9.20] and adopting the following parameters:

$$\alpha = C_T^* s^* \qquad [9.24]$$

the transmissibility function can be expressed under the form:

$$T^* = \frac{\theta^*(L,p)}{\theta^*(0,p)} = [\cosh(s^* L) + \frac{D}{C} \sinh(s^* L)]$$

Replacing D/C by its value calculated versus the applied torque:

$$T^* = \frac{1}{\cosh(s^* L) + \frac{p^2 \cdot J_1}{\gamma} \sinh(s^* L)} \qquad [9.25]$$

If one works in the harmonic regime, in [9.24] p= jω and the transmissibility function becomes:

$$T^* = \frac{1}{\cos \varsigma^* - \gamma \varsigma^* \sin \varsigma^*} \qquad [9.26]$$

$$\text{with } \phi = \frac{J_1}{J_s} = \frac{J_1}{\rho L I_p} \quad m^* = [\frac{\rho I_p \omega^2}{C_T}]^{1/2} \qquad [9.27]$$

I is the inertia of half the sample. The inverse of the transmissibility function is written as:

$$\gamma = \frac{J_a}{I} = \frac{J_a}{\rho L I_p} \quad \varsigma^* = \omega L[\frac{\rho I_p}{C_T}]^{1/2} \qquad [9.28]$$

$$\varsigma^* = p + jq$$

$$\left.\begin{aligned} \eta_R &= \cos p \cdot \cosh q - \gamma p \sin p \cdot \cosh q + \gamma q \cos p \cdot \sinh q \\ \eta_I &= \sin p \cdot \sinh q + \gamma p \cos p \cdot \sinh q + \gamma q \sin p \cdot \cosh q \end{aligned}\right\} \qquad [9.29]$$

Newton-Raphson's method, applied to the coupled equations to solve the dynamic viscoelastic problem, is presented elsewhere (see [CHE 10], Chapter 5).

The following equations are useful to obtain complex shear modulus for a solid propellant:

$$G^* = \mu^* = \mu_R + j\,\mu_I \; ; \; C_T^* = C_R + jC_R \qquad [9.30]$$

$$\mu^* = \frac{C_T^*}{bh^3\beta_T(\frac{b}{h})} \qquad [9.31]$$

The real part μ_R and imaginary part μ_I are, respectively:

$$\mu_R = \frac{1}{h^3 b\alpha(\frac{b}{h})} \cdot \left[\frac{(p^2 - q^2)\rho I_p\ \omega^2 L^2}{(p^2-q^2)^2 + 4p^2q^2}\right] \qquad [9.32]$$

$$\mu_R = \frac{1}{bh^3\beta_T(\frac{b}{h})} \cdot \left[\frac{(p^2 - q^2)\rho I_p\ \omega^2 L^2}{(p^2+q^2)^2}\right]$$

$$\mu_I = \frac{1}{h^3 b\alpha(\frac{b}{h})} \cdot \left[\frac{-pq\rho I_p\ \omega^2 L^2}{(p^2-q^2)^2+4p^2q^2}\right] \qquad [9.33]$$

$$\mu_I = \frac{1}{bh^3\beta_T(\frac{b}{h})} \cdot \left[\frac{-2pq\rho I_p\ \omega^2 L^2}{(p^2+q^2)^2}\right]$$

where $\beta_T\left(\frac{b}{h}\right)$ is the Saint Venant's warping function, which is a function of the flatness of the cross-section (defined as the ratio of the width b to thickness h, see equation [9.C.1], Appendix 9C).

$$\tan\delta_\mu = \frac{\mu_I}{\mu_R} = \frac{-2pq}{p^2-q^2} \qquad [9.34]$$

9.10.2. *Solution of the viscoelastic problem*

As the complex shear modulus is deduced from the transmissibility function, electronic equipment with a discrete Fourier transform is necessary. Repeated impact tests allow better results to be obtained. Figures 9.15(a) and (b) present absolute values of shear modulus and damping ratio at various sample temperatures. Figure 9.15(a) shows regular curves while the curves concerning the damping ratio (Figure 9.15(b)), seem to vary in a random manner.

Figure 9.15 gathers only portions of curves at various temperatures which are suited to apply the translation technique of the William-Landel-Ferry's method. Figure 9.16 presents the translation factor and the shear modulus over three decades of frequency.

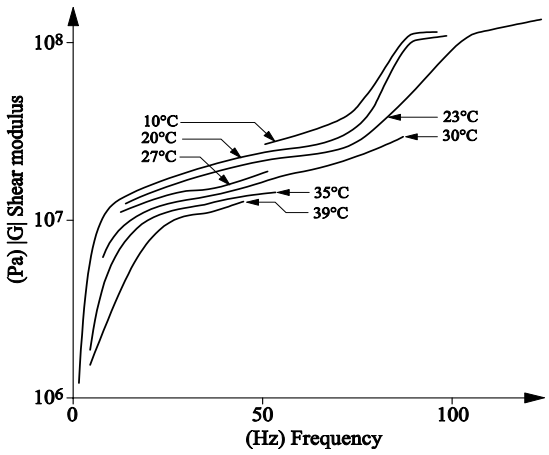

Figure 9.15(a). *Complex shear modulus (expressed in absolute value) of solid propellant versus frequency at various temperatures*

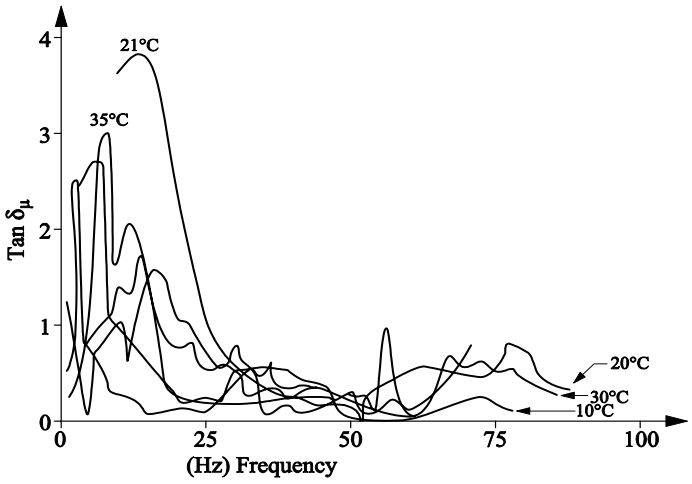

Figure 9.15(b). *Damping ratio of solid propellant at various temperatures versus frequency*

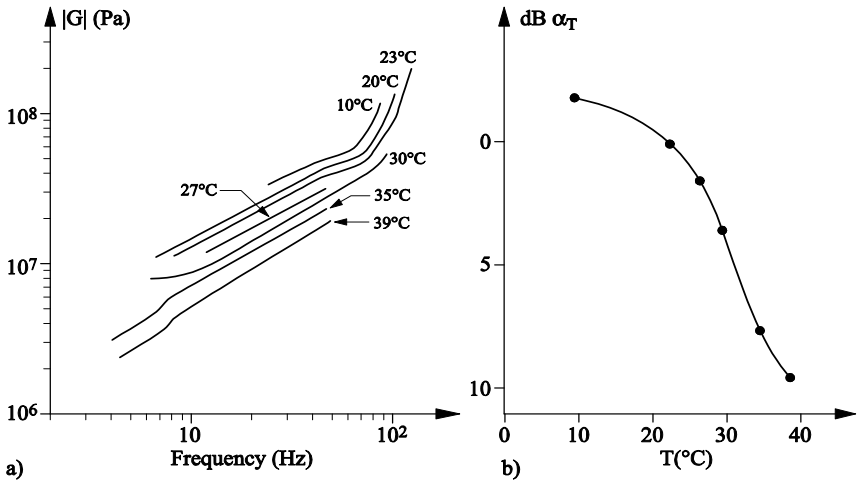

Figure 9.16. *(a) Complex shear modulus of solid propellant (absolute value) gathered in view of application of translation William-Landel-Ferry's method; (b) translation coefficient a_T versus frequency*

In logarithmic coordinates, the curve in Figure 9.15 clearly shows two distinct slopes in the transition zone.

9.10.3. *Closed form expression of complex shear modulus of solid propellant using versus frequency*

We have previously presented [CHE 10] two methods to express complex modulus in the form of a quotient of two polynomials, or by using fractional derivatives. Those methods are purely graphical.

9.10.3.1. *Expression of complex shear modulus $G^*(f) = \mu^*(f)$*

The curves presented here [CHE 10] for a solid propellant presents some analogies with those obtained by Osaki, Tamura *et al*. [OSA 65].[7]

Then expression of complex shear modulus $G^*(f) = \mu^*(f)$ is given by equation [9.35]:

$$\mu^*(p = j\omega) = \left(\frac{p+4.6}{p+7.5}\right)\left(\frac{p+10.3}{p+37}\right)\left[\left(\frac{p+70}{p+90}\right)\left(\frac{p+115}{p+125}\right)\right]^{4.2}. 2.10^8 \text{ Pa.} \qquad [9.35]$$

7 There are two classes of methods; the fractional derivative method and the polynomial method which are explained in details in [CHE 10], Chapter 3.

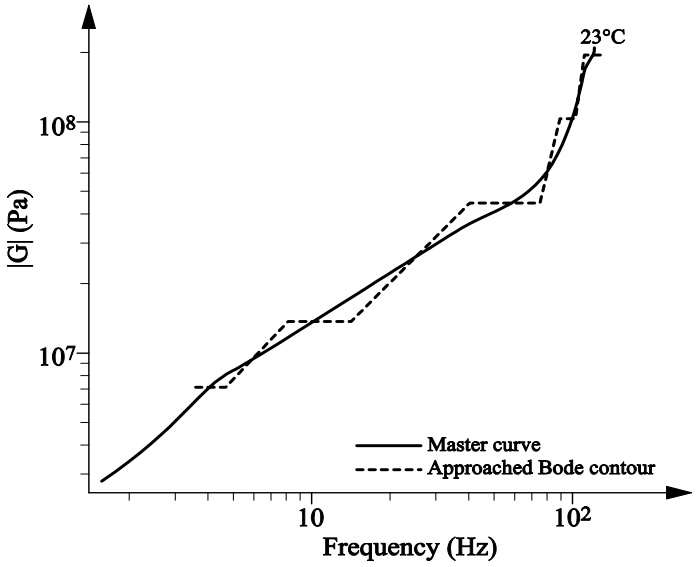

Figure 9.17. *Master curve of complex shear modulus of solid propellant versus frequency; reference temperature: 20°C*

9.11. Concluding remarks

9.11.1. *Metallic materials*

9.11.1.1. *Isotropic materials*

– With the exception of special composite materials fabricated for specific applications, the elastic shear modulus of isotropic materials does not vary with frequency in isothermal tests in the case of square cross-sections, due to the relative wave number being defined as the ratio of the wave number on the half of the sample thickness.

– Shear wave dispersion is relatively weak but cannot be neglected at high frequency. The dispersion curve varies with the flatness coefficient of the rod sample.

– If the experimenter has the latitude to choose a square cross-section of the sample rod, the dispersion curve approaches that of a circular cross-section very closely, at least for the first elastodynamic mode.

9.11.2. *Composite materials*

– In the case of special composite materials which have been fabricated for advanced applications with high strength and high modulus, fibers must not be assimilated with those of metallic materials. Young's modulus in the direction of fibers is high while shear moduli are weak and, in practice, of the order of those concerning high polymers. The ratio E_3/G_{13} or E_3/G_{23} is very high (3 direction of fiber) and this ratio strongly influences wave dispersion.

– The flatness of the cross-section (δ = (width b)/(thickness h)) also plays an important role in the dispersion curve trend.

– Utilization of scientific research devoted to the dispersion phenomena of isotropic rod samples cannot be extended to composite materials without taking precautions [CHE 10].

9.11.3. *Experimental set-up*

The experimental set-up must be adapted to specific application, say a simple industrial characterization or for dispersion studies, the frequency range not always being the same.

With regard to material characterization for industrial applications, short or long samples should be used, with apparatus devised for low frequency.

The dispersion curves used should be a free sample with a lightweight special transducers and special suspensions which do not influence the measurements at high frequency (i.e. a contact string sample).

For low damping materials, two methods have been presented for viscoelastic characterization. See [CHE 10], Chapters 4 and 11 for theory and in [CHE 10], Chapter 8 for measurement techniques. William-Landel-Ferry's method is one of the possibilities on the condition that the applicability of the translation method is valid with combined parameters of temperature and frequency.

9.12. Bibliography

[CHE 79] CHEVALIER Y., CHEMOUIL J., ESTEOULE C, *Dynamic tests on solid propellant composite,* SNPE contract N° 30/78/D, in French, 1979.

[CHE 10] CHEVALIER Y., VINH, J.T., (eds), *Mechanics of Viscoelastic Materials and Wave Dispersion*, ISTE, London and John Wiley & Sons, New York, 2010.

[EST 79] ESTEOULE C., *Dynamic tests on Solid Propellant,* Research final report to obtain engineer degree, ISMCM Saint Ouen France, December 1979.

[FER 69] FERRY J. D., *Viscoelastic Properties of High Polymers* (Second edition), John Wiley & Sons, New York, USA, Chapter 17, pp. 510-556, 1969.

[NUG 76] NUGUES M., VINH J.T., *Torsion Vibration of Anisotropic Rod of Composite Material,* Comptes rendus de l'Académie des sciences, série B, pp. 289-292 in French, 1976.

[ONO 78] ONOBIONO J. *On the Dynamic Torsion of Anisotropic Rod with Circular Cross Section,* PhD; dissertation, University of Paris VI, 27 April, 1978.

[REN 05] RENARD J. *Elaboration, Microstructures et Comportement des Matériaux à Matrice Polymère*, Lavoisier-Paris, (2005).

[OSA 65] OSAKI K., TAMURA M., KURATA M.AND KOTAKA T. "The behaviour of materials under combined steady and oscillatory shear", *J. Phys. Chem*. Vol.69, pp. 4183, 1965.

[VIN 86] VINH T., CHEMOUIL J., ESTEOULE C., *Impact Tests on Solid Propellant*, Sciences et technique de l'Armement, Memorial de l'Artillerie française, Tome 61, 3rd Fascicule, pp. 201-235, 1986.

[VIN 90] VINH T., CHEVALIER Y., LE NIZHERY D., *Course on Dynamic Characterization of Composite Materials,* Saint Ouen France, 1990.

9.13. Appendix 9A. Choice of equations of motion

The objective of this appendix is to present a quick overview on the choice of appropriate equations of motion, taking into account the important parameters depending either on sample geometrical parameters or on elastic (or viscoelastic) moduli of the tested sample.

9A.1. *Circular cross-section*

If we have the latitude of choice of cross-section geometry, a circular cross-section is the easiest and favourable choice. There is no restriction on the frequency range and no wave dispersion, at least for the first elastodynamic vibration mode. The equation of motion is reduced to an elementary second degree one:

$$G\frac{\partial^2\theta}{\partial z^2} = \rho\frac{\partial^2\theta}{\partial t^2} \qquad [9.A.1]$$

where G is shear modulus, and ρ density.

In the case of an isotropic material and where the z axis is a symmetry axis, G should be replaced by G_{xz} or G_{yz}. In the case of an isotropic material and where z is

not coincident with the symmetry axis of the material, there is a warping phenomenon and equation [9.A.1] is not valid.

On practical grounds, if the material is an artificial multilayered composite, there is difficulty in fabricating a circular cross-section sample.

9A.2. *Square cross-section*

If the dynamic torsion tests are limited to the evaluation of shear modulus, a square cross-section presents interesting properties. In this case, only the first elastodynamic torsional mode is retained and wave dispersion is absent, on the condition that the sample axis is coincident with the symmetry axis of the material.

9A.3. *Rectangular cross-section*

A rectangular cross-section sample is the easiest one to fabricate. Inevitably, the phenomenon of warping occurs in torsion tests and must be taken into account.

9A.3.1. *Important geometrical parameters*

There are two parameters:

(a) slenderness =h (thickness) or b (width)/ L(length);

(b) flatness δ = b(width)/h(thickness).

Wave dispersion is strongly dependent on δ and varies in the same sense.

9A.4. *Ratio of Young's modulus to shear modulus*

For an isotropic material, the importance of this ratio is taken into account in the equations of motion via the influence of components of displacement other than the shear component. In other words, the displacement field has more than one component and the formulation of a torsion problem gives rise to various hypotheses adopted at the beginning. In increasing order of complexity we can have various equations of motion, as follows.

9A.4.1. *Saint Venant's theory for the formulation of adopted static torsion*

Saint Venant's theory gives rise to a second order elementary equation of motion:

$$C_T \frac{\partial^2 \theta}{\partial z^2} = \rho I_p \frac{\partial^2 \theta}{\partial t^2} \qquad [9.A.2]$$

with $C_T = C[G_{yz}, G_{xz}, \beta_T(b,h,G_{yz}/G_{xz})]$, where C_T is the rod torsional stiffness expressed via Saint Venant's theory (describing the warping of the cross-section). β is a parameter function of thickness, h, and width, b, of the rod and the two shear moduli G_{xz} and G_{yz} (see[CHE 10], Chapter 5).

9A.4.2. *More elaborate Saint Venant's theory* [8]

This takes into account axial displacement. Coupled motion exists: where the torsional angle θ and axial displacement w(x,y) each give rise to a second order equation of motion with a coupling term.

The decoupled equation of motion is of the fourth order.

9A.4.3. *Other theories*

Barr's theory, with a correcting term obtained by evaluating an asymptotic value of the phase velocity (which tends to Rayleigh's wave velocity) should be mentioned.

9A.5. *Special experimental studies of wave dispersion phenomenon*

In this chapter, an experimental set-up using an exciter and transducers has been adopted and is commercially available. The mechanical system is easy to realize with a very long rod.

The objective of this study has been not only to evaluate shear modulus but also to compare, eventually, the validity of different proposed equations. The phenomenon of warping is described, not by Saint Venant's theory, but by a more elaborated theory proposed by Engstrom.

9.14. Appendix 9B. Complementary information concerning formulae used to interprete torsion tests

9B.1. *Quick overview of Saint Venant's theory applied to the problem of dynamic torsion*

9B.1.1. *Quasi-static theory of torsion*

The choice of an appropriate theory depends on the objective chosen at the beginning. If the choice is confined to calculation of shear modulus at a lower frequency range, inside of which wave dispersion is not taken into account, then

8 See Nugues's theory, [NUG 76], which is applicable to composite anisotropic material.

Saint Venant's theory (valid for the static study of the warping function) is applicable.

A second order theory of rod torsion is adopted:

$$\rho I_p \frac{\partial^2 \theta}{\partial t^2} = C_T \frac{\partial^2 \theta}{\partial z^2} \qquad [9.B.1]$$

In [9.B.1] C_T is expressed versus the warping function $\phi_w(x,y)$, where x,y are the cordinates of the section.

The boundary conditions give rise to a wave number β equation which is necessary to calculate the shear modulus G_{xz} and G_{yz}.

9B.1.2. *Higher order theory*

The hypothesis adopted above in 9B.1.1 is that the projection of the cross-section rotates rigidly in its plane. It is not valid for higher elastodynamic modes. The displacement component along the rod axis w(z,t) was written above in [9.B.2]; see also [CHE 10], Chapter 5, Appendix 5B:

$$w(z,t)=\xi(z,t)\phi_w(x,y) \qquad [9.B.2]$$

Using the Hamilton principle, we obtain equations of motions as well as boundary conditions. Two Euler's equations are obtained:

$$\frac{P_1}{S_{33}} \frac{\partial^2 \xi}{\partial z^2} - \rho P_1 \frac{\partial^2 \xi}{\partial t^2} - K_a \xi - K_a \frac{\partial \theta}{\partial z} = 0$$
$$-\rho I_p \frac{\partial^2 \theta}{\partial t^2} + I_a \frac{\partial^2 \theta}{\partial z^2} - K_a \frac{\partial \xi}{\partial z} = m \qquad [9.B.3]\ [9.B.4]$$

where m designates distributed torque on the rod lateral surface. Coefficients in [9.B.3] are expressed in terms of ϕ_w and coodinates x,y. m=0 for a free lateral surface.

An uncoupling operation is possible to reduce [9.B.3] [9.B.4] into an equation of the fourth degree:

$$\left(\rho^2 \frac{P_1 I_p}{K_a}\right) \frac{\partial^4 \theta}{\partial t^4} + \left(\frac{P_1 I_a}{S_{zz} K_a}\right) \frac{\partial^4 \theta}{\partial z^4} - \left[\frac{\rho P_1 I_p}{S_{zz} K_a} + \frac{\rho P_1 I_a}{K_a}\right] \frac{\partial^4 \theta}{\partial z^2 \partial t^2} + \rho I_p \frac{\partial^2 \theta}{\partial t^2} - (I_a - K_a) \frac{\partial^2 \theta}{\partial z^2} = 0 \qquad [9.B.5]$$

We recognize that the last two terms in [9.B.5] are equation [9.B.1], an elementary equation. It has been demonstrated that (I_a-K_a) is reduced to C_T as in [9.B.1]. The third term is called the longitudinal inertia term. The first two terms correspond to an axial stress correcting term.

9B.1.2.1. Boundary conditions

There are two boundary conditions at each end in Figure 9.1. This is coherent with the fourth order equation of motion [9.B.5].

For z=0 at the middle of the sample, there is no axial displacement: $\delta\xi=0$.

The second boundary condition is a prescribed external torque

$$J_0 \frac{\partial^2 \theta}{\partial t^2} = 2\left[I_a \frac{\partial \theta}{\partial z} - K_a \xi \right] \qquad [9.B.6]$$

J_0 is the mandrel polar inertia. Coefficient 2 can be explained by adoption of excitation at the middle at the sample.

For z = $\pm$L there is no warping stress at both ends; $\frac{\partial Z}{\partial z} = 0$.

The second boundary condition concerns the additional lever inertia which corresponds to prescribed torque:

$$- J_L \frac{\partial^2 \theta}{\partial t^2} = I_a \frac{\partial \theta}{\partial z} - K_a \xi \qquad [9.B.7]$$

Boundary conditions include the torsion angle $\theta(z,t)$ and also the second variable $Z(z,t)$.

It can be demonstrated that the same equation of motion [9.B.5] is valid for variable $\xi(z,t)$ in which $\theta(z,t)$ is replaced by $\xi(z,t)$. We can express these two functions versus characteristic functions (two trigonometric functions and two hyperbolic functions). There are consequently eight coefficients to determine and we have at our disposal only four boundary conditions. Fortunately, there are relationships between the two sets of four coefficients given by equation [9.B.4]. Details concerning closed form expressions of $\xi(z,t)$ and $\theta(z,t)$ as well as calculations of eigenvalues of the rod submitted to torsional vibration are given in [CHE 10], Chapter 5 and Appendixes 5B and 5D.

Computer programs can be elaborated and a trial and error method is used to obtain eigenvalues.

9.15. Appendix 9C: details concerning the $\beta_T(c)$ function in the calculation of rod stiffness C_T

The expression of rod stiffness C_T is:

$$C_T = G_{yz}\, hb^3\, \beta_T(c) = G_{xz}\, bh^3\, \beta_T(1/c) \qquad [9.C.1]$$

with b width, h thickness, z direction of the rod axis, and c is defined as:

$$c = \frac{h}{b}\sqrt{\frac{G_{xz}}{G_{yz}}} \qquad [9.C.2]$$

The series giving $\beta_T(c)$ is the following:

$$\beta_T(c) = \left[\frac{1}{3} - \frac{64}{c\pi^5}\sum_{k=1,3,5\ldots}\frac{1}{k^5}\tanh\frac{k\pi c}{2}\right] \qquad [9.C.3]$$

Series [9.C.3] is quickly convergent taking into account the fifth power of odd integer k in the denominator of the quotient inside the brackets.

c	$\beta_T(c)$	c	$\beta_T(c)$	c	$\beta_T(c)$
1	0.14058	14	0.31833	27	0.325553
2	0.22868	15	0.31933	28	0.325553
3	0.26832	16	0.32020	29	0.325833
4	0.28081	17	0.32098	30	0.326092
5	0.29132	18	0.32166	31	0.326561
6	0.29832	19	0.32228	32	0.326771
7	0.30332	20	0.32283	33	0.326972
8	0.30707	21	0.323786	34	0.327161
9	0.30999	22	0.323786	35	0.327338
10	0.31232	23	0.324202	36	0.327502
11	0.31423	24	0.324581	37	0.327657
12	0.31588	25	0.324984	38	0.327815
13	0.31717	26	0.325255	39	0.327953
				40	0.328092

Table 9C.1. *The warping function $\beta_T(c)$, where c is given by [9.C.2]*

9.16. Appendix 9D. Compliments concerning the solution of equations of motion with first order theory

The higher order theory of torsion is presented, given in detail elsewhere by Chevalier and Vinh [CHE 10] in Chapter 5. We give here the principal equations and formulae which enable the reader to conceive the computer code giving eigenvalue results with boundary conditions inherent to the torsion apparatus presented in Figure 9.1, i.e. pseudo-clamping in the middle of the sample and additional torsional inertias at both ends.

9D.1. *Displacement field*[9]

$$\begin{aligned} u(z,t) &= -\theta(z,t)\, y \\ v(z,t) &= \theta(z,t)\, x \\ w(z,t) &= \xi(z,t)\, \phi_w(x,y) \end{aligned} \qquad [9.D.1]$$

$\xi(z, t)$ replaces the torsion angle θ in the component w(z,t) adopted in elementary theory. We then have two functions $\theta(z, t)$ and $\xi(z, t)$ to evaluate instead of one function $\theta(z, t)$. $\phi_w(x, y)$ is the warping function supposed to be identical to the warping function in static torsion.

9D.2. *Relations between two sets of coefficients*

Harmonic solutions for $\theta(z, t) = A(z) \exp(j\omega t)$ and for $\xi(z, t) = B(z) \exp j\omega t$ are adopted.

Introducing [9D1] into [9.B.4] we obtain for [9.B.4]:

$$\rho I_p \omega^2 A + \frac{I_a L^2}{C_T} \frac{\partial^2 A}{\partial z^2} - \frac{K_a L^2}{C_T} \frac{\partial B}{\partial z} = 0 \qquad [9.D.2]$$

By dividing all the terms in [9.D.2] by C_T / L^2 we obtain:

9 The projection of the cross-section rotates rigidly in its plane. That is the simplifying assumption in the framework of Saint Venant's theory.

$$\frac{\rho\, I_p\, \omega^2\, L^2}{C_T} A + \frac{I_a\, L^2}{C_T} \frac{\partial^2 A}{\partial z^2} - \frac{K_a\, L^2}{C_T} \frac{\partial B}{\partial z} = 0 \qquad [9.D.3]$$

It is convenient to adopt the following dimensionless parameters:

$$v_1 = \frac{\rho\, I_p\, \omega^2\, L^2}{C_T} \qquad v_2 = \frac{P_1}{I_p\, L^2}$$

$$v_3 = \frac{I_p\, \omega^2}{s_{33}\, C_T} \qquad v_4 = \frac{I_a}{C_T} \qquad [9.D.4]$$

C_T is the torsion rigidity relating torque to angle. It is equal to:

$$C_T = (I_a - K_a)$$

$$\left(\frac{P_1\, I_a}{s_{33}\, K_a}\right)\beta^4 + \left[+\left(\frac{\rho\, P_1\, I_p}{s_{33}\, K_a} + \frac{\rho\, P_1\, I_a}{K_a}\right)\frac{\omega^2}{L^2} - \frac{I_a - K_a}{L^2}\right]\beta^2 - \rho\, I_p\, \omega^2 + \frac{\rho^2 P_1 I_p}{K_a}\omega^4 = 0$$

$$\beta^4 - \left[\frac{v_4 - 1}{v_2 v_3 v_4} - \frac{v_1 v_2 (v_3 + v_4)}{v_2 v_3 v_4}\right]\beta^2 - v_1\left[\frac{v_4 - 1}{v_2 v_3 v_4} - v_1 \frac{v_2}{v_2 v_3 v_4}\right] = 0 \qquad [9.D.5]$$

In the second equation in [9.D.5] dimensionless parameters adopted in [9.D.4] are used.

In the bi-squared equations in β, the sum of the roots is positive and their product is negative.

The solutions for A (z) and B(z), see [CHE 10] equations [5.62] and [5.68], can be written as:

$$A(z) = A_a \cos h \frac{\beta_1 z}{L} + B_a \sin h \frac{\beta_1 z}{L} + C_a \cos \frac{\beta_2 z}{L} + D_a \sin \frac{\beta_2 z}{L} \qquad [9.D.6]$$

$$B(z) = A_b \cosh \frac{\beta_1 z}{L} + B_b \sinh \frac{\beta_1 z}{L} + C_b \cos \frac{\beta_2 z}{L} + D_b \sin \frac{\beta_2 z}{L}$$

The set of coefficients A_a, B_a, C_a, D_a is to be evaluated by the four boundary conditions, two at each end. Coefficients of B(z) are obtained as shown in the following section.

9D.3 *Equations giving the two sets of coefficients A_a,B_a,C_a,D_a deduced from the four boundary conditions*

Equation [9.B.6] has proven to be convenient for expressing coefficients with index b as functions of a coefficients with index a. The following two coefficients concern non-dimensional polar inertia at the free end of the rod and the polar inertia of the mandrel in the rod middle.

$$\eta_L = \frac{J_L}{\rho L I_p} = 1/\gamma \qquad \eta_0 = \frac{J_0}{\rho L I_p} \qquad [9.D.7]$$

The denominators of the parameters above represent the polar inertia of half of the rod , J_m, and the polar inertia J_a is the polar inertia of the lever at the free end.

For z=L the prescribed torque T is $J_L \frac{\partial^2 \theta}{\partial t^2}$ so:

$$\eta_L \frac{v_1}{L v_4} A = \left(\frac{\partial A}{\partial z} - B \frac{v_4 - 1}{v_4} \right) \qquad [9.D.8]$$

$$\frac{\partial Z}{\partial z} = 0 \text{ (no warping stress)}$$

For z=0

$$\eta_0 \frac{v_1}{L v_4} A = 2\left[\frac{\partial A}{\partial z} - B \frac{v_4 - 1}{v_4} \right] \qquad [9.D.9]$$

9D.4. *Evaluation of coefficients in [9.D.6]*

With the parameters v_1, v_2, v_3, v_4 in [9.D.4], equation [9.D.2] has the following form:

$$v_1 A + v_4 \frac{\partial^2 A}{\partial z^2} L^2 - L^2 (v_4 - 1) \frac{\partial B}{\partial z} = 0 \qquad [9.D.10]$$

[9.D.7] relates variable Θ to Z as follows:

$$A_b = B_a \frac{v_1 + v_4 \beta_1^2}{\beta_1 L (v_4 - 1)}, \qquad B_b = A_a \frac{v_1 + v_4 \beta_1^2}{\beta_1 L (v_4 - 1)}$$

$$C_b = - D_a \frac{(v_1 - v_4 \beta_2^2)}{\beta_2 L (v_4 - 1)} \qquad D_b = C_a \frac{(v_1 - v_4 \beta_2^2)}{\beta_2 L (v_4 - 1)}$$

Or

$$A_b = r_a B_a, \qquad B_b = r_a A_a$$

$$C_b = - s_a D_a, \qquad D_b = s_a C_a$$

[9.D.11]

In [9.D.11], β_1 , β_2 are the two roots of the characteristic equations [9.D.5]

9D.5. *Equations in* A_a , B_a , C_a , D_a *deduced from the four boundary conditions*

[9.D.11] (or [5.D.4] in [CHE 10]) is proved to be convenient to express coefficients with index b as functions of a coefficient with index a.

The two following coefficients concern the non-dimensional polar inertia at the free end and the polar inertia of the mandrel in the middle.

$$\eta_L = \frac{J_L}{\rho I_p L} = \frac{1}{\gamma}. \qquad \eta_0 = \frac{J_0}{\rho I_p L} \qquad [9.D.12]$$

The denominators (m) of η_L and η_0 in [9.D.12] represent the polar inertia of half of the rod. γ is used for elementary torsional equation of motion.

a) For z = L

The prescribed torque T, [5.B.13], at the end z =L of the sample is $-J_L \frac{\partial^2 \theta}{\partial t^2}$, then:

$$\eta_0 \frac{v_1}{v_4 L} A = 2 \left[\frac{\partial A}{\partial z} - B \frac{v_4 - 1}{v_4} \right] \qquad [9.D.13]$$

Z = 0

Bringing the harmonic solution, sections 9.D.2 into [9.D.9] and [9.D.13] the following set of equations are obtained (see [CHE 10], Appendix 5.D)

$$A_a \left[- \frac{\eta_L}{v_4} \frac{v_1}{L} \cos h \beta_1 + \sin h \beta_1 \left(\frac{\beta_1}{L} - \frac{v_4 - 1}{v_4} r_a \right) \right] +$$

$$B_a \left[- \frac{\eta_L}{v_4} \frac{v_1}{L} \sin h \beta_1 + \cos h \beta_1 \left(\frac{\beta_1}{L} - \frac{(v_4 - 1)}{v_4} r_a \right) \right] +$$

$$C_a \left[- \frac{\eta_L}{v_4} \frac{v_1}{L} \cos \beta_2 - \sin \beta_2 \left(- \frac{\beta_2}{L} - \frac{v_4 - 1}{v_4} s_a \right) \right] +$$

$$D_a \left[- \frac{\eta_L}{v_4} \frac{v_1}{L} \sin \beta_2 + \cos \beta_2 \left(\frac{\beta_2}{L} + \frac{v_4 - 1}{v_4} s_a \right) \right] = 0$$

$$A_a r_a \beta_1 \cos h \beta_1 + B_a r_a \beta_1 \sin h \beta_1 + C_a s_a \beta_2 \cos h \beta_2 + D_a s_a \beta_2 \sin h \beta_2 = 0$$

$$A_a \left[- \frac{\eta_m \, v_1}{v_4 \, L} \right] - 2 \, B_a \left[\frac{\beta_1}{L} - \frac{v_4 - 1}{v_4} \, r_a \right]$$
$$- 2 \, D_a \left[\frac{\beta_2}{L} + \frac{v_4 - 1}{v_4} \, s_a \right] + C_a \left[- \frac{\eta_m \, v_1}{v_4 \, L} \right] = 0$$

$$B_a \, r_a - D_a \, r_a = 0 \qquad [9.D.14]$$

The four equations in [9.D.14] enables us to establish the determinant of coefficients of A_a, B_a, C_a, D_a presented under matricial form.

$$\begin{bmatrix} 0 & \frac{v_1 + v_4 \beta_1^2}{\beta_1} & 0 & \frac{v_1 - v_4 \beta_2^2}{\beta_2} \\ \eta_0 & -\frac{2}{\beta_1} & \eta_0 & \frac{2}{\beta_2} \\ \left(v_1 + v_4 \beta_1^2\right) \cosh \beta_1 & \left(v_1 + v_4 \beta_1^2\right) \sinh \beta_1 & \left(v_1 - v_4 \beta_2^2\right) \cosh \beta_1 & \left(v_1 - v_4 \beta_2^2\right) \sinh \beta_2 \\ \left(\eta_L \cosh \beta_1 + \frac{\sinh \beta_1}{\beta_1}\right) & \left(\eta_L \sinh \beta_1 + \frac{\cosh \beta_1}{\beta_1}\right) & \left(\eta_L \cosh \beta_2 + \frac{\sinh \beta_2}{\beta_2}\right) & \left(\eta_L \sinh \beta_2 - \frac{\cosh \beta_2}{\beta_2}\right) \end{bmatrix} = 0$$

[9.D.15]

By setting this determinant to zero we obtain the characteristic equation in β_1, β_2.

There are two unknowns β_1 and β_2, but the sum of the squares of β_1 and β_2 in the bisquared equation is:

$$\beta_1^2 + \left(j \, \beta_2\right)^2 = \beta_1^2 - \beta_2^2 = \frac{v_4 - 1}{v_2 \, v_3 \, v_4} - \frac{v_1 \, v_2 \, \left(v_3 + v_4\right)}{v_2 \, v_3 \, v_4} \qquad [9.D.16]$$

and the product is:

$$\left(\beta_1^2\right) \bullet \left(j \, \beta_2^2\right) = - \beta_1^2 \, \beta_2^2 = - v_1 \left[\frac{v_4 - 1}{v_2 \, v_3 \, v_4} - \frac{v_1 \, v_2}{v_2 \, v_3 \, v_4} \right] \qquad [9.D.17]$$

[9.D.15, 16, 17] are three equations in β_1, β_2, v_1.

The following notations are adopted to simplify the writing of equations:

$$S_1 = v_2\ v_3\ v_4\ ,\ S_2 = \frac{v_4 - 1}{s_1}\ ,\ S_3 = \frac{v_2}{s_1}\ ,\ S_4 = \frac{v_2\ (v_3 + v_4)}{s_1} \qquad [9.D.18]$$

Eliminating β_1, we obtain:

$$v_1^2\ S_3 - v_1\ \left(S_2 + \beta_2^2\ S_4\right) + \left(\beta_2^4 + S_2\ \beta_2^2\right) = 0 \qquad [9.D.19]$$

Effecting [9.D.15] and eliminating β_1, a new equation in $v_1$and v_2 is obtained (see [CHE 10], relation [5.D.14]).

$$\frac{-2\ \eta_L}{\left[v_1\ (S_2 - v_1\ S_3)\right]^{1/2}}\ \left[v_1^2 + v_4\ v_1\ (S_2 - v_4\ v_1) - v_4^2\ v_1\ (S_2 - v_1\ S_3)\right]$$

$$+ \sin \beta_2\ \cosh\left[\beta_2^2 + S_2 - v_1\ S_4\right]^{1/2}$$

$$\bullet v_4 \sqrt{\Delta}\ \frac{\left(2 - \eta_L \eta_0 \beta_2^2\right)\ \left[v_1 + v_4\ \left(\beta_2^2 + S_2 - v_4\ S_4\right)\right]}{\beta_2\ \left[v_1\ (S_2 - v_1\ v_1\ S_3)\right]^{1/2}}$$

$$- \sin \beta_2\ \sin h\left[\beta_2^2 + S_2 - v_1\ S_4\right]^{1/2} \bullet$$

$$\frac{\left[\eta_L\ (S_2 - v_1\ S_4)\right]\ \left[v_1^2 + v_4\ v_1\ (S_2 - v_1\ S_4) - v_4^2\ v_1\ (S_2 - v_1\ S_4)\right]}{v_1\ (S_2 - v_1\ S_3)}$$

$$- \cos\ \beta_2\ \sin h\left[\beta_2^2 + S_2 - v_1\ S_4\right]^{1/2} \bullet$$

$$\frac{(v_1 - v_4)\ \beta_2^2 \bullet \sqrt{\Delta}\ v_4\ \left[2 + \eta_L\ \eta_0\ \left(\beta_2^2 + S_2 - v_1\ S_4\right)\right]}{\left[v_1\ (S_2 - v_1\ S_3)\right]^{1/2}\ \left[\beta_2 - S_2 - v_1\ S_4\right]^{1/2}}$$

$$- \cos\ \beta_2\ \cos h\left[\beta_2^2 + S_2 - v_1\ S_4\right]^{1/2} \bullet$$

$$\left\{ \begin{array}{l} \dfrac{2\,\eta_0\,v_4^2\,\Delta}{\left[v_1\,(S_2 - v_1\,S_3)\right]^{1/2}} \\ + \dfrac{\eta_L\left[2\,v_1^2 + v_1\,v_4\,(S_2 - v_1\,S_4) + v_4^2\left(\beta_2^4 + \left(\beta_2^2 + S_2 - v_1\,S_4\right)\right)^2\right]}{\left[v_1\,(S_2 - v_1\,S_3)\right]^{1/2}} \end{array} \right\} = 0 \quad [9.D.20]$$

[9.D.19] and [9.D.20] constitute a set of two equations whose unknowns are v_1 and β_2. It would be possible to solve those equations to obtain v_1 and β. The calculations are tedious. It is better to solve them numerically.